J Mater Sci: Mater Electron (2016) 27:6076–6087
DOI 10.1007/s10854-016-4533-2

CrossMark

Effect of nano-TiO_2 addition on microstructural evolution of small solder joints

Z. L. Li[1] · G. Y. Li[1] · L. X. Cheng[1] · J. H. Huang[1]

Received: 1 November 2015 / Accepted: 14 February 2016 / Published online: 22 February 2016
© Springer Science+Business Media New York 2016

Abstract The influence of TiO_2 addition on the interfacial reaction in Sn–3.0Ag–0.5Cu solder joints with the pad size of 200 μm was investigated in this study. The microstructure of the solder joints and the interfacial intermetallic layers were analyzed by scanning electron microscope. Results show that both the thickness and grain size of the intermetallic compound (IMC) decreases when TiO_2 is added. The Sn–3.0Ag–0.5Cu–0.1TiO_2 solder exhibits the most prominent effect in retarding interfacial IMC growth and refining IMC grain size. It is observed that the scallop morphology became more faceted in shape compared with the large size Cu/solder interface, where the Cu_6Sn_5 grains appear to be round shape no matter the reflow time is long or short. The cause might be due to the change in interfacial energy between the molten solder and Cu_6Sn_5 phase, which is highly correlated with the Cu concentration profile near the interface in the side of the liquid solder.

1 Introduction

With the fast development of the miniaturization of the electronic packaging, the properties and behaviors of the small solder joint are obviously different from those of the large solder joint. Large solder joints contain a large number of randomly oriented grains at the interface and the characteristic behavior of the solder joints describes the average performance of these grains [1]. As a consequence, large solder joint can usually be considered as isotropic and homogeneous. However, the small solder joints are different from that and may contain only a few grains at the interface [1, 2]. Their performance is therefore expected to shift from the characteristic of a polycrystalline material. In such cases the individual grains play an important role in the behavior of the solder joints. In addition to the grains and their orientation, with the size and volume of solder joints become miniature continuously, the proportion of the brittle IMC to the whole solder joint will increase which can cause the higher probability of brittle interface failure of solder joint interconnections [3].

Many studies have been carried out to investigate the size effect on the interfacial reaction in solder joints. Kao et al. [4] studied the effect of the Cu concentration in solder, solder volume, and temperature on soldering reactions between Sn–Ag–Cu solder and Ni under bump metallization for the joint diameter of 375 μm. They found that as the residual apparent Cu concentration in the solder decreases and the solder volume reduces, the type of intermetallic compound changes from $(Cu, Ni)_6Sn_5$ to $(Ni, Cu)_3Sn_4$. Chan et al. investigated the interfacial reactions between Sn–3.5Ag–0.5Cu solder ball and Cu pad. The solder balls of 760 and 500 μm in diameter were soldered on the Cu pad with the size of 600 μm in diameter surrounded by a solder mask [5, 6]. They concluded that the mean thickness of the intermetallic for solder with smaller volume is thicker than that of the bigger solder balls. Park et al. [7] reported that the thickness of interfacial Cu_6Sn_5 layer increases and as the size of solder balls decreases. In the case of small solder ball, Cu dissolution rate into molten solder was faster than large solder ball due to its high pad area/solder volume ratio. Fast Cu dissolution into molten solder promotes the IMC growth. Yang et al. [8] studied Sn–3.0Ag–0.5Cu and Sn–3.5Ag solder balls with different diameters were soldered on Cu substrates with an

✉ G. Y. Li
phgyli@scut.edu.cn

[1] School of Electronic and Information Engineering, South China University of Technology, Guangzhou 510641, China

opening diameter of 250 μm. They found that a larger Cu concentration gradient results in smaller Cu_6Sn_5 grains and more consumption of Cu substrate. To determine whether a size effect exists for creep properties of solder joints or not, Yin [9] characterized the creep behaviors of small Sn–3.0Ag–0.5Cu lead-free solder joints with 200 and 400 μm in diameter. They concluded that the joints with a larger size exhibit a much higher steady-state creep rate and a shorter creep lifetime than the smaller joints.

To get solder joints with higher microstructure stability and better mechanical properties, a potentially viable and economically affordable approach is to incorporate appropriate second phase particles in the solder matrix such as TiO_2, Al_2O_3, ZrO_2 and $SrTiO_3$ [10–17]. Previous work reveals that adding a small amount of TiO_2 into Sn–Ag–Cu solder can visibly improve the wetting and mechanical properties of the solder for large solder joint [10, 16–19]. Nasir et al. [17] investigated the physical performances of low-silver SAC lead-free composite solder reinforced with different composition TiO_2. Compared with monolithic SAC solder alloy, the results showed that distribution of TiO_2 increased the hardness of the composite solders. Tang et al. [18] studied the growth kinetics of the IMC between composite solder and Cu substrate. The morphologies and thickness of Cu_6Sn_5 IMC change with the change of reflowing time and nano-TiO_2 addition. The microstructure and hardness of SAC and SAC-0.1TiO_2 solder joints with a diameter of 0.76 mm were compared by Gain [19]. After the addition of TiO_2 nanoparticles, IMC particles appeared with a fine microstructure and retarded the growth rate of IMC layers at the interfaces. And the composite solder joints displayed a higher hardness. Although a lot of work focuses on the addition of nano-TiO_2 into lead-free solder for the improvement of properties of the solder joint, most of works focus on the bigger solder joint. As interfacial morphology and IMC growth have a big influence on the reliability of small solder joint, it is still necessary to investigate the interfacial IMC growth mechanism in detail for the small solder joints. This paper focuses on studying the effects of TiO_2 additive on the IMC formation and growth kinetics of the IMC layer in small solder joints. The size effect is explored by comparing the interfacial microstructure, IMC growth kinetics and IMC grain morphology of the small solder joints with big solder joints.

2 Experimental

Composite solders were prepared by mechanically dispersing different weight percentages (0, 0.05, 0.1, 0.3, and 0.6 wt%) of TiO_2 nano-powder into Sn–3.0 wt%Ag–0.5 wt%Cu solder paste. The mixture was blended mechanically for at least 40 min to achieve a uniform distribution of TiO_2 nanopowder. Figure 1 shows the image of the TiO_2 nano-particles

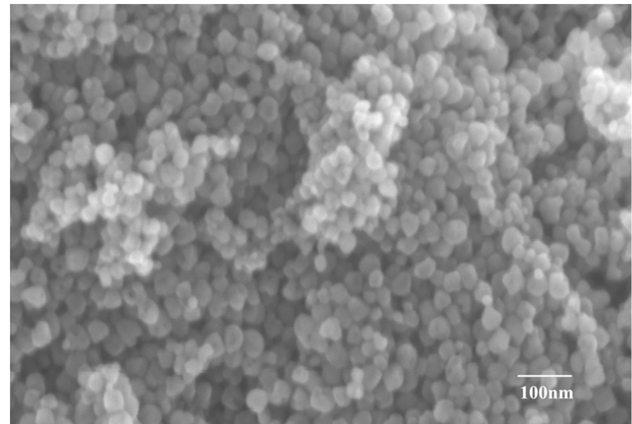

Fig. 1 FEG-SEM image of the TiO_2 nano-particles

taken by a field emission gun scanning electron microscope. The average diameter of the spherical TiO_2 nano-particles is 20 nm. The Cu pad with Au surface finish used in this study has an opening diameter of 200 μm. The Sn–3.0Ag–0.5Cu–xTiO_2 solders were carefully applied on the pads and Cu substrate using a stainless steel stencil, and were formed with an infrared reflow oven. The diameter of the solder joint for 200 μm Cu pad is about 500 μm. Figure 2 shows micrograph of the cross section view and top view of the Cu pad. In order to characterize the existence of nano-TiO_2 particles in lead free solder, EDX and XRD analysis were carried out for the Sn–3.0Ag–0.5Cu–0.6TiO_2 solder joint and the results are shown in Fig. 3. Both EDX and XRD results confirmed that TiO_2 phase is existed in the solder.

The typical temperature profile is shown in Fig. 4 and the reflow peak temperature is 250 °C. The dwell times above liquidus temperature were set to be 30, 60, 120, 240, 480, and 1200 s, respectively. The longer reflow dwell times of 240, 480, and 1200 s in this work were specially designed to study the effects of TiO_2 addition on the IMC growth kinetics of the interfacial reaction.

For metallographic observations, specimens were first mounted in crystal glue and cross-sectioned perpendicularly to the solder joint. They were then successively ground down to 1000 grit with silicon carbide paper cooled with flowing water. Polishing was performed using 5 μm Al_2O_3 suspension followed by 0.25 μm diamond paste. The specimens were then etched in a dilute solution of 2 % concentrated hydrochloric acid (HCl), 6 % concentrated nitric acid (HNO_3), and 92 % H_2O for a few seconds. To observe the microstructural evolution of the intermetallic grains, the solder alloys on the top of the IMC were chemically etched away by using 30 % (by volume) nitric acid. The etching time depended on the thickness of the remaining solder to be removed.

SEM with backscattered model was used to observe the microstructural morphology of IMC. EDX and XRD were

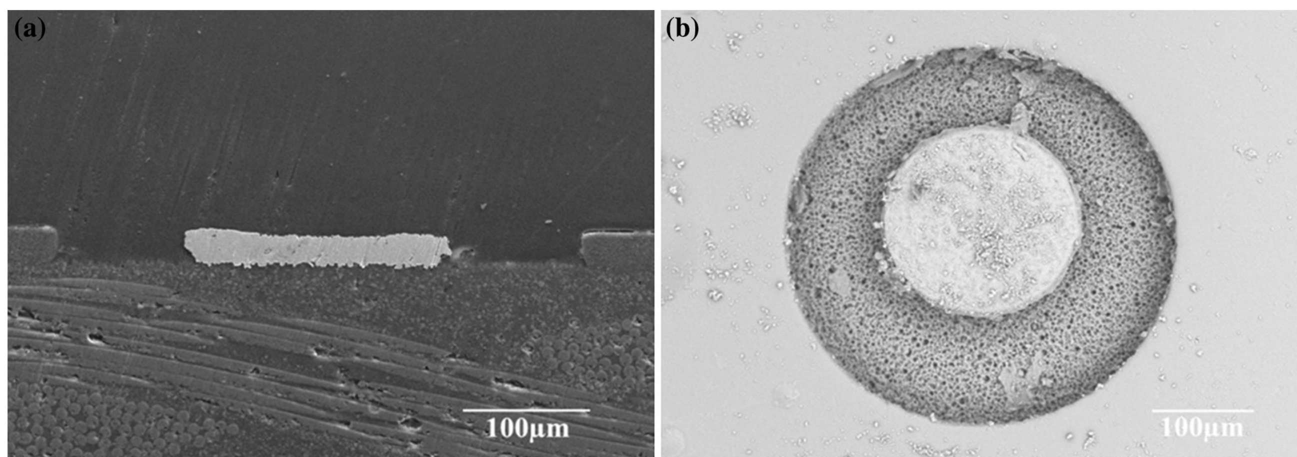

Fig. 2 Micrograph of the Cu pad: **a** cross section view, **b** top view

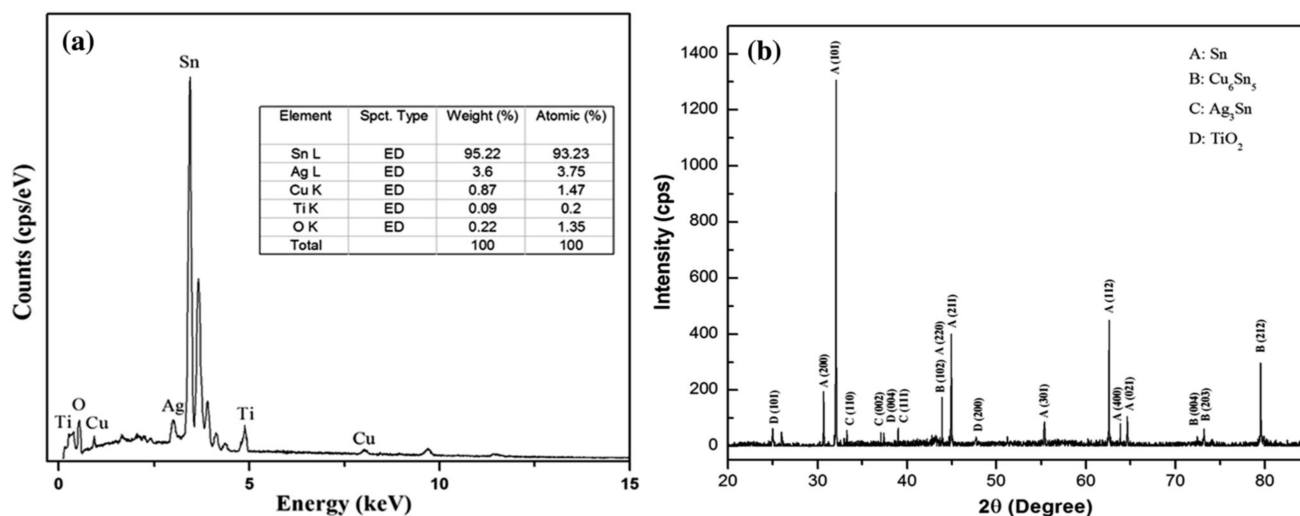

Element	Spct. Type	Weight (%)	Atomic (%)
Sn L	ED	95.22	93.23
Ag L	ED	3.6	3.75
Cu K	ED	0.87	1.47
Ti K	ED	0.09	0.2
O K	ED	0.22	1.35
Total		100	100

Fig. 3 EDX (**a**) and XRD (**b**) analysis of composite solder matrix for the Sn–3.0Ag–0.5Cu–0.6TiO_2 solder joint

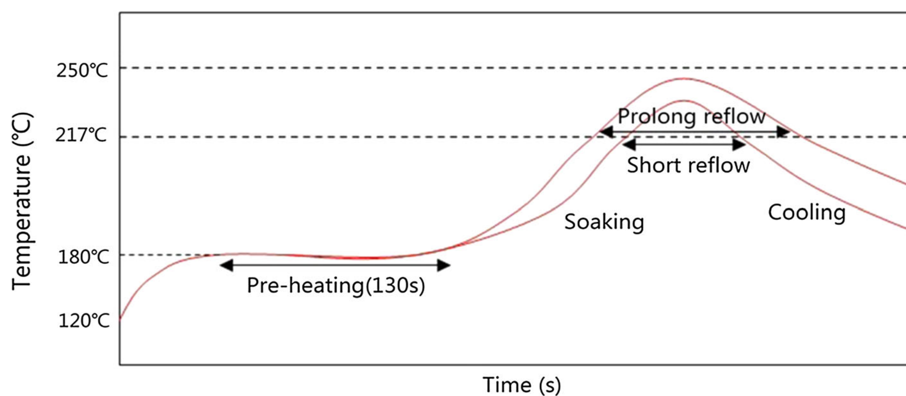

Fig. 4 Typical reflow temperature profile

used to characterize the composition of the samples. The mean thickness measurement of the IMC was performed using SEM and image analysis. For each condition, three samples were prepared. For each sample, four SEM photographs were taken at different positions. The area and length of the IMC layer for each photograph were measured, and the area divided by length is defined as the thickness of the IMC. The data obtained from twelve measurements were used to calculate an average thickness for each condition.

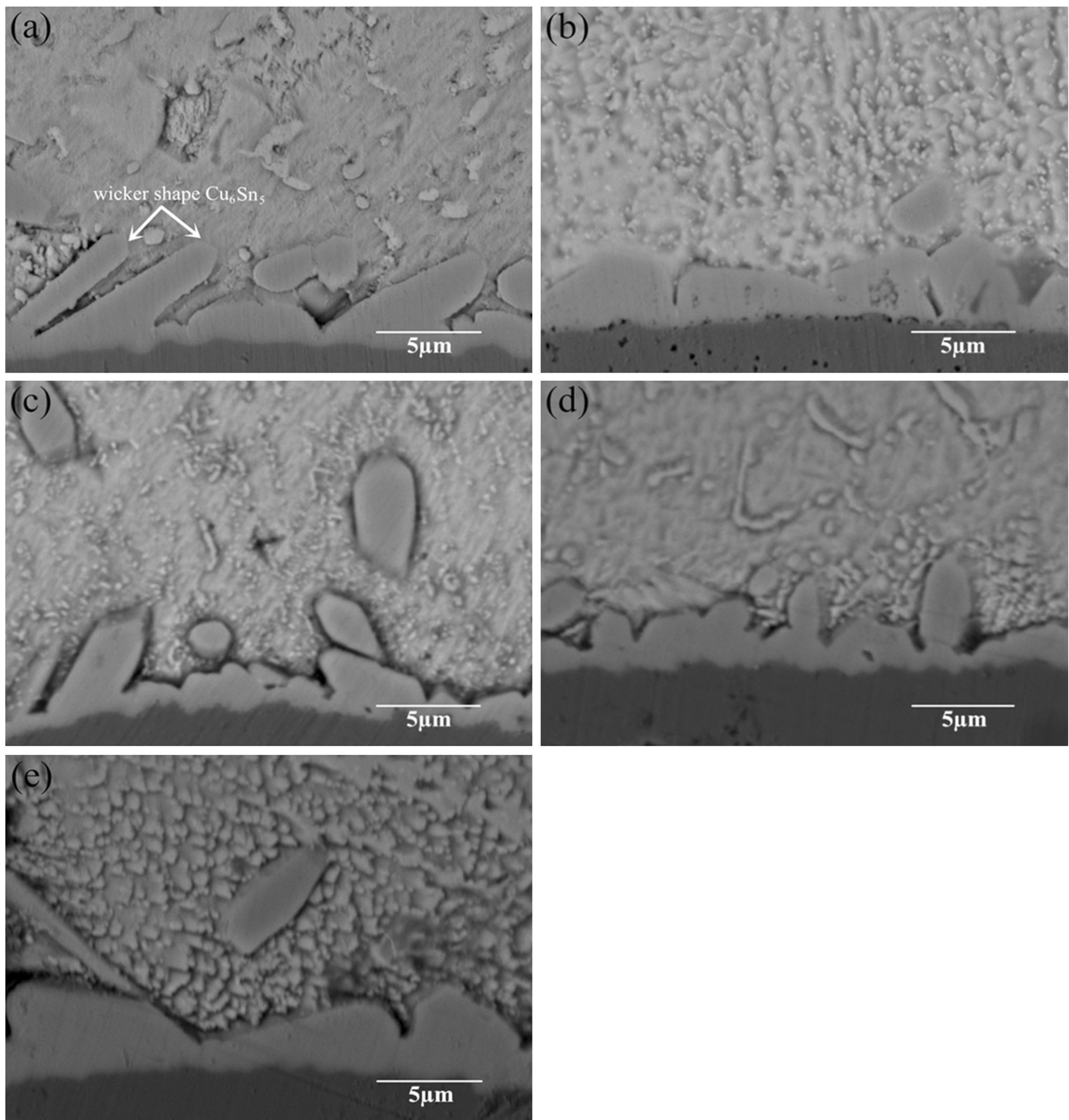

Fig. 5 SEM micrographs of cross-sectional view of Sn–3.0Ag–0.5Cu–xTiO_2 solder joints reflowed for 60 s for 200 μm Cu pad. **a** x = 0, **b** x = 0.05, **c** x = 0.1, **d** x = 0.3, **e** x = 0.6 wt%

3 Results and discussion

3.1 IMC growth

Figures 5 and 6 show the typical SEM micrographs of the cross-sectional view of the solder joints for 200 μm Cu pad and Cu substrate for the reflow dwell time of 60 s, respectively. Figure 5 clearly shows that the Cu_6Sn_5 phase grows as wicker scallop-like grain into the solder matrix, and results in a very rough interfacial morphology between the solder and the IMC. With an increase in weight percentage of TiO_2 nano-particles, the morphology of the Cu_6Sn_5 IMC layer changes from an wicker scallop-like to a continuous rough scallop-like, as shown in Fig. 5b–e. These longer IMCs could induce brittle fracturing at the interface and provide crack initiation sites. It is worth to

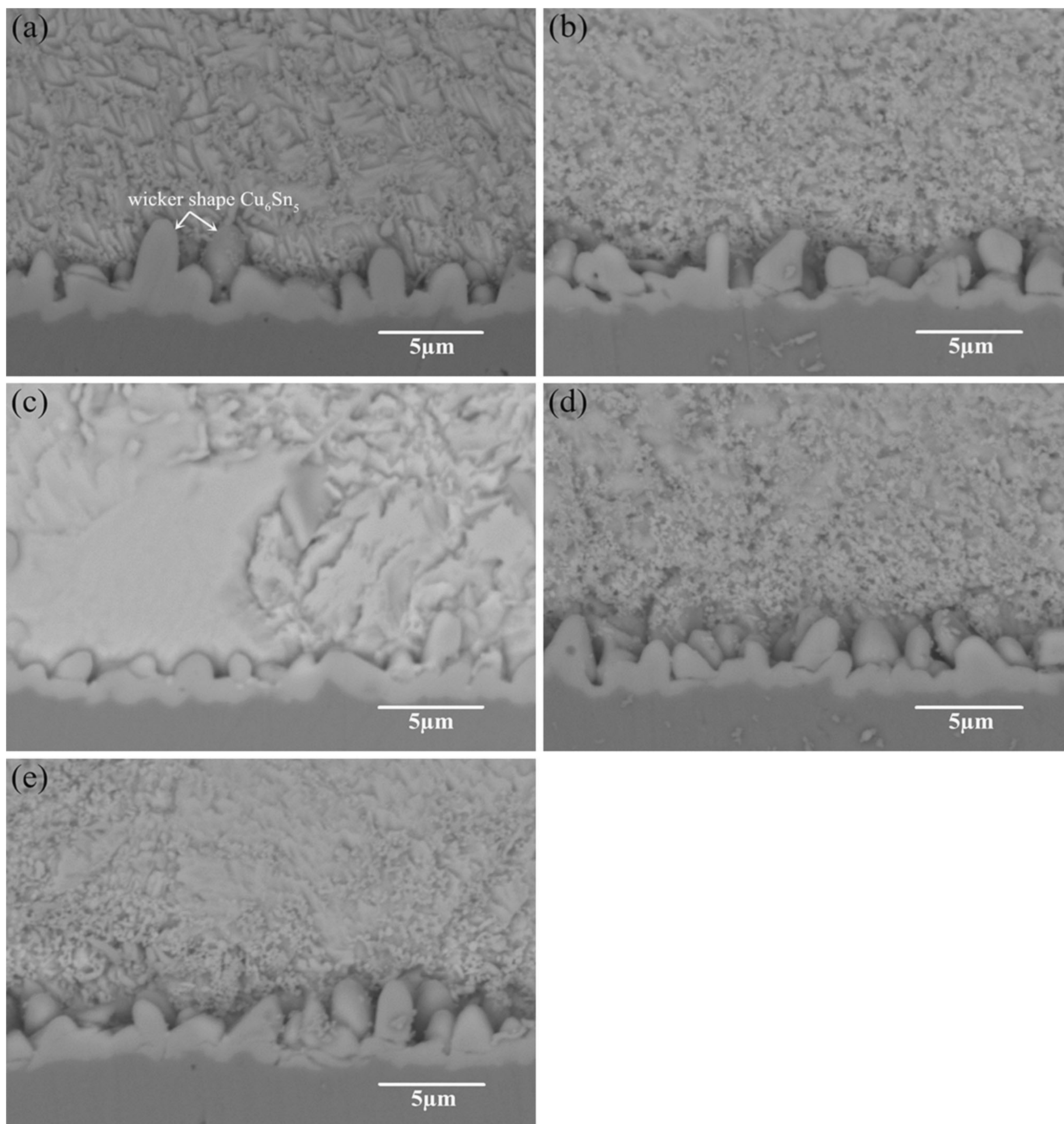

Fig. 6 SEM micrographs of cross-sectional view of Sn–3.0Ag–0.5Cu–xTiO_2 solder joints reflowed for 60 s for Cu substrate. **a** x = 0, **b** x = 0.05, **c** x = 0.1, **d** x = 0.3, **e** x = 0.6 wt%

point out that the formation of the wicker shape Cu_6Sn_5 IMC emerging from the scallop tops is related to a local concentration increase in copper, which results in the IMC growing into the solder matrix by the reaction of tin with the copper [20, 21]. The wicker shape Cu_6Sn_5 IMC layer might be adverse to the reliability of the solder joints. This similar phenomenon has been observed in the large solder joints, as shown in Fig. 6.

A column chart shown in Fig. 7 summarizes the IMC thicknesses of the solder joints for 200 µm Cu pad and Cu substrate reflowed for 60 s. For small solder joints, the thicknesses of IMC in TiO_2-containing samples are thinner than that of the TiO_2-free sample. When the weight percentage of TiO_2 approaches to 0.1 wt%, the IMC thickness drops from 2.65 to 2.32 µm. This result reveals that for the same reflow dwell time, IMC thickness decreases with the

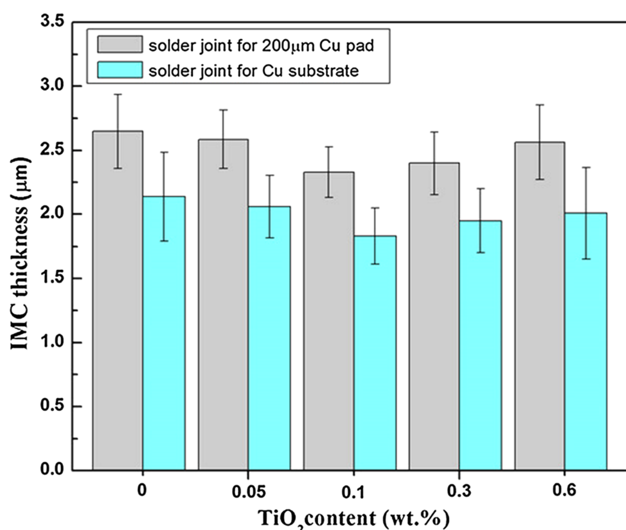

Fig. 7 IMC thickness for different TiO_2 compositions reflowed for 60 s

increase of TiO_2 proportion, and the downward trend persists until the weight percentage of TiO_2 approaches to about 0.1 wt%. Beyond this amount, the IMC thickness increases slightly, but is still thinner than that of the TiO_2-free solder joints. This result reveals that adding TiO_2 could inhibit the growth of IMC in liquid-state reactions. However, the thickness of the IMC is much thicker than the solder joints for Cu substrate, as shown in Fig. 7. The IMC thickness increases from 1.83 to 2.32 μm for the TiO_2 weight percentage of about 0.1 wt%. According to the model of Kao [22], for smaller solder joints, the Cu concentration in the solder rises faster than the larger ones. So the smaller joints could experience the effect of the higher Cu concentrations for longer periods of time which make the scallops grow larger. This might be the reason why the IMC thickness of the small solder joints is much thicker than that of the large solder joints.

3.2 Growth kinetics of the IMC formation

As shown in Fig. 7, the optimized TiO_2 concentration is about 0.1 wt%. In this study, only this concentration is selected to analyze the IMC growth kinetics. Figure 8 shows the typical SEM micrographs of the cross-sectional view of the Sn–3.0Ag–0.5Cu–0.1TiO_2 solder joints for the reflow dwell times of 30, 60, 120, 240 and 1200 s respectively. By increasing the reflow time, the IMC layer thickness is substantially increased. After forming the layer structure of Cu_6Sn_5 phase between the solder and Cu pad, a thin layer of the Cu_3Sn compound with a dark contrast was found at the interface between the Cu_6Sn_5 and Cu, as shown in Fig. 8e. The formation of Cu_3Sn can be attributed to two types of mechanisms: decomposition of Cu_6Sn_5, i.e., $Cu_6Sn_5 + 9Cu \rightarrow 5Cu_3Sn$, when the Cu_6Sn_5 was thick, and formation by a Cu–Sn reaction, i.e., $3Cu + Sn \rightarrow Cu_3Sn$ [23].

A column chart shown in Fig. 9 summarizes the IMC thicknesses in solder joints reflowed for different dwell time. As expected, the thickness increases with the increase in reflow time. The thicknesses of IMC in TiO_2-containing and TiO_2-free solder joints show almost no difference for reflow dwell time of 30 s. However, for the longer reflow dwell times, the IMC layer of the TiO_2-containing samples is thinner than that of the TiO_2-free samples. When the reflow dwell time prolongs to 1200 s, the IMC thickness drops from 7.19 to 6.4 μm. This result reveals that adding TiO_2 could inhibit IMC growth.

The suppression of the growth of Cu_6Sn_5 IMC layer by the addition of TiO_2 nano-particles can be explained by the adsorption theory. According to the theory of adsorption [20, 24, 25], the surface free energy of Cu_6Sn_5 grains is:

$$\sum_k \gamma^k_{(c)} A_k = \sum_k \left(\gamma^k_{(0)} - RT\int_0^c \frac{\Gamma^k}{c}dc\right)A_k$$
$$= \sum_k \gamma^k_{(0)} A_k - RT\sum_k A_k \int_0^c \frac{\Gamma^k}{c}dc \rightarrow \min$$

where Γ^k is the amount of TiO_2 nano-particles adsorption at Cu_6Sn_5 particle k, c is the concentration of TiO_2 nano-particles, R is the ideal gas constant, T is the absolute temperature, $\gamma^k_{(c)}$ is the surface tension of Cu_6Sn_5 particle k with the adsorption of TiO_2 nano-particles, $\gamma^k_{(0)}$ is the surface tension of Cu_6Sn_5 particle k without adsorption of TiO_2 nano-particles and A_k is the area of Cu_6Sn_5 particle k. Given that the volume of IMC is constant, the surface energy of the planes must be kept to be minimum in the equilibrium state. Here, $\sum_k \gamma^k_{(0)} A_k$ is assumed to be constant because it is independent of the concentration of TiO_2 nano-particles. So the term $\sum_k A_k \int_0^c \frac{\Gamma^k}{c}dc$ should be maximized, which implies that the surface energy of Cu_6Sn_5 grains decreases with an increase in the amount of adsorption of TiO_2 nano-particles. Gibbs reported that the surface energy reduction will decrease the growth velocity of the Cu_6Sn_5 grains [20, 25, 26]. Hence, the growth rate of the whole of the Cu_6Sn_5 IMC layer was suppressed.

To determine the time dependence of IMC growth, a general empirical equation, the power law, is employed to describe the relationship between IMC thickness and reflow time [27]:

$$y = kt^b$$

where y is the average IMC thickness, t is the time, k is the growth parameter, and b is the growth exponent of IMC layer. k and b are determined by analyzing the measured IMC thickness using curve-fitting. In this work, IMC thickness

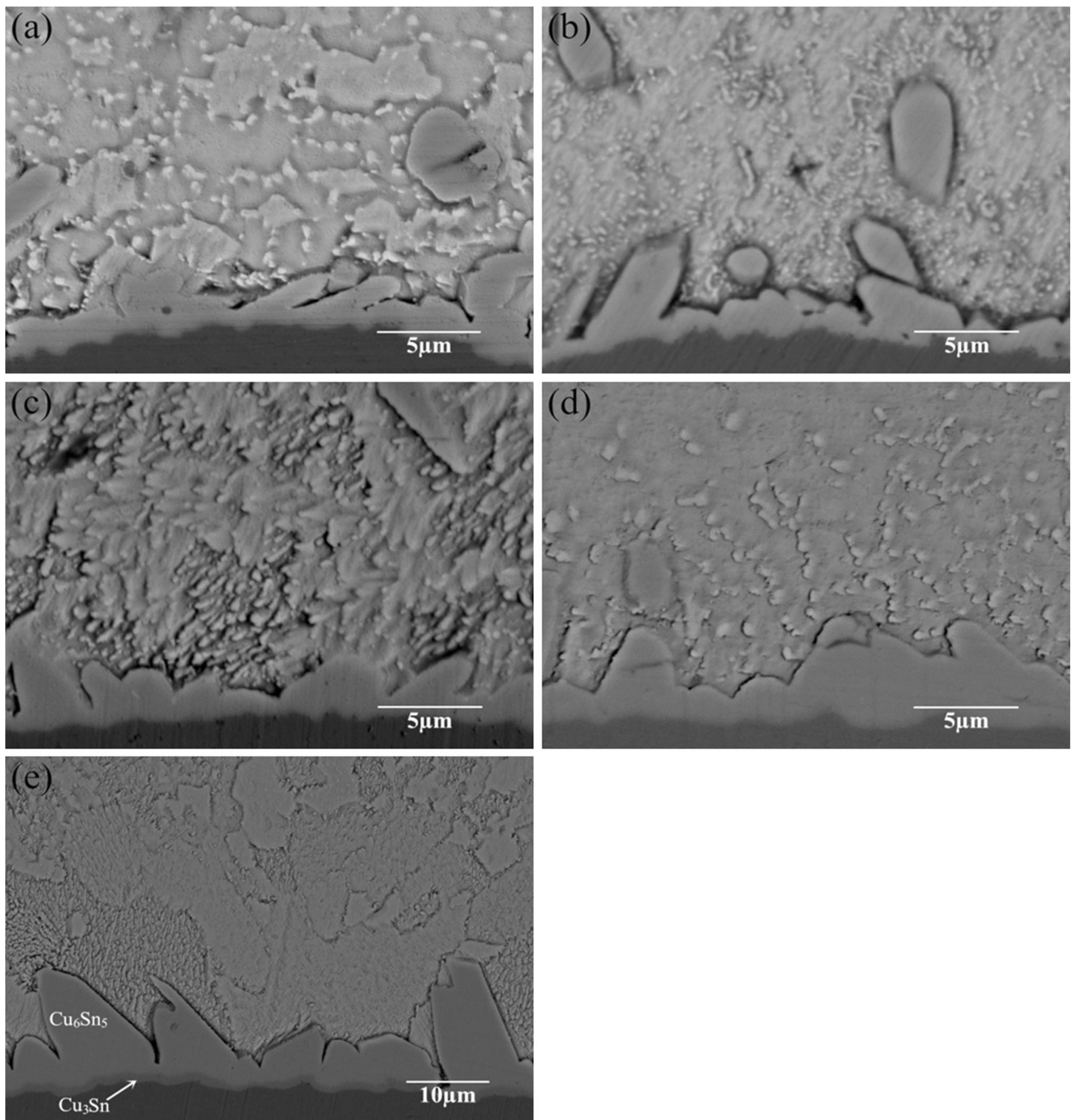

Fig. 8 Backscattered SEM micrographs of cross-sectional view of Sn–3.0Ag–0.5Cu–0.1TiO_2 solder joint reflowed for **a** 30 s, **b** 60 s, **c** 120 s, **d** 240 s and **e** 1200 s

growth exponent is used to describe the kinetics of IMC growth because the IMC formation and growth controlled by atomic diffusion and interfacial reaction. The curve fitting plots of the thickness of IMC are shown in Fig. 10. It fits the experimental data quite well. The IMC layer growth exponents b of TiO_2-free solder joints and Sn–3.0Ag–0.5Cu–0.1TiO_2 solder joints are 0.356 and 0.338, respectively. It can be found that the growth exponent b is between 1/3 and 1/2. So the mechanism of IMC growth in the soldering reaction is a combination of the interfacial reaction-controlled growth and diffusion-controlled growth [28]. This observation is similar with big solder joints [29].

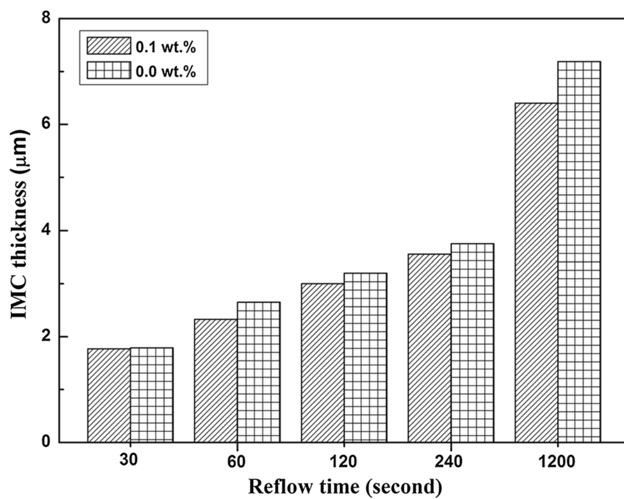

Fig. 9 IMC thickness versus reflow time for different TiO_2 compositions

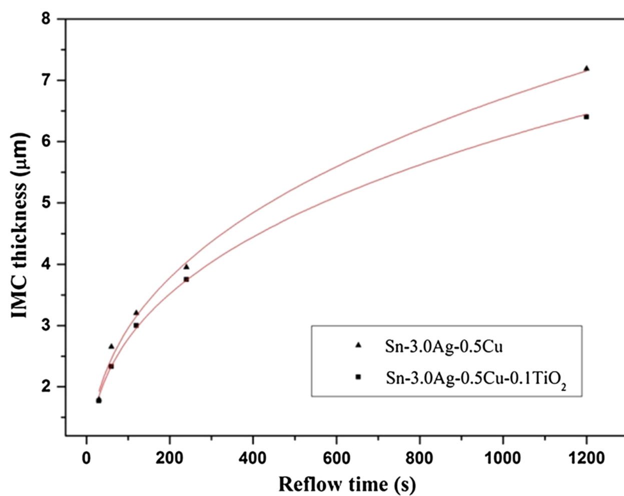

Fig. 10 Curve fitting of the IMC thickness for Sn–3.0Ag–0.5Cu and Sn–3.0Ag–0.5Cu–0.1TiO_2 solder joints

3.3 The evolution of Cu_6Sn_5 grains

In this study, the typical Sn–3.0Ag–0.5Cu–0.1TiO_2 solder joint is selected to discuss the evolution of the Cu_6Sn_5 grains. SEM micrographs of the top view of IMC layer of Sn–3.0Ag–0.5Cu–0.1TiO_2 solder joints for different reflow dwell times are shown in Fig. 11, after etching the solder away. It can be observed that the interfacial compound formed is the same, yet the morphology is different. Figure 11a is a SEM image of Cu_6Sn_5 grains for the dwell time of 30 s. It is obvious that the Cu_6Sn_5 grains display highly faceted rather than rounded scallop type structure, and distribute homogeneously across the whole Cu surface. Compared with the samples reflowed for 30 s, when the reflow time increases to 60 s, faceted scallops were observed all over the sample along with few round scallops, as shown in Fig. 11b. And the size of the Cu_6Sn_5 grains increases slightly. However, when the reflow time is increased to 120 s, the morphology of the Cu_6Sn_5 grains becomes different, as shown in Fig. 11c. The faceted scallops Cu_6Sn_5 grains gradually become round scallop grains. Further increasing the reflow time up to 1200 s, as shown in Fig. 11d, the number of Cu_6Sn_5 grains with faceted interface increases again and the Cu_6Sn_5 grains become much larger.

In general, Cu_6Sn_5 is the first phase to form at the liquid solder/Cu interface. The first stage of the reaction is the dissolution of Cu to liquid solder, until the solder becomes supersaturated with Cu more or less uniformly at the liquid solder/Cu interface. According to the description of Laurila et al. [30], when Cu comes into contact with molten Sn it starts to dissolve rapidly. Initially, the dissolution is a non-equilibrium process and locally very high concentrations of Cu can be realized in the very vicinity of the liquid solder/Cu interface. Figure 12 shows the micrograph and EDX spectrum of the solder joint reflowed for 30 s at the IMC/solder interface.

The distributions of experimental Cu concentration at the IMC/solder interface analyzed by EDX for different reflow time are summarized in Table 1. As the reaction reflow time is increased, the concentration of Cu at the IMC/solder interface decreases, which is consistent with the literature [8, 30]. When the reflow time is 30 s, the concentration of Cu is much higher than solution limit. With the reflow time increasing to 120 and 1200 s, the concentration of Cu is lower than solution limit. It may be due to the continuous IMC layer formed at the interface, which block the Cu fast diffusing through the fragmented IMC channel. The IMC barrier reduces the atomic flux of Sn and Cu elements, slowing down their reaction. This means that diffusion of metals is slowed down by an increase in diffusion path length created by the IMC barriers and reduction in concentration of metals in the system [31].

As is reported by Suh, morphology of the scallop-type Cu_6Sn_5 was dependent to the composition of the solder. The scallop morphology became more faceted when the composition was further away from the eutectic composition [32]. And the experimentally determined composition of the Sn–Ag–Cu ternary eutectic is about Sn–3.5Ag–0.9Cu at 217 °C [30]. It can be seen from Table 1 that the value of Cu concentration at the IMC/solder interface is very close to the eutectic composition for the samples reflowed for 120 s. So it is possible that the evolution of top-view morphology of the Cu_6Sn_5 correlated to the reflow time is due to the change of Cu concentration at the IMC/solder interface. According to literature reported by Tu [33], the distribution of alloy elements at the Cu_6Sn_5/solder interface has an strong effect on the interfacial energy between the molten solder and Cu_6Sn_5. And the

Fig. 11 SEM micrographs of top view of IMC layer of Sn–3.0Ag–0.5Cu–0.1TiO$_2$ solder joints reflowed for **a** 30 s, **b** 60 s, **c** 120 s and **d** 1200 s for Cu pad of 200 μm in diameter

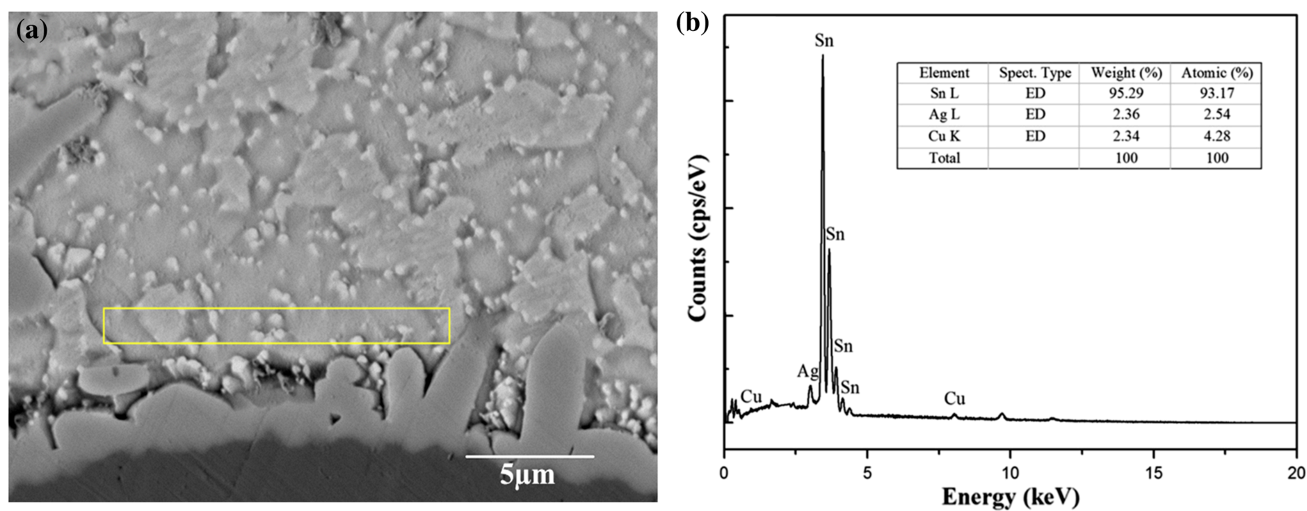

Fig. 12 Micrograph and EDX spectrum for Sn–3.0Ag–0.5Cu–0.1TiO$_2$ solder joints reflowed for 30 s at the IMC/solder interface: **a** micrograph, **b** EDX spectrum

change of interfacial energy further affects the morphology. When the composition is far away from the eutectic composition, the interfacial energy is more anisotropic which makes the scallop morphology highly faceted. As the composition gradually close to the eutectic composition, the interfacial energy of scallops tends to be more

Table 1 Average Cu concentration of Sn–3.0Ag–0.5Cu–0.1TiO_2 for 200 µm Cu pad at the IMC/solder interface for different reflow time

Reflow time (s)	30	60	120	1200
wt%	2.34	1.48	0.99	0.61

isotropic. Then the scallop morphology became more rounded.

To compare the grain morphology of the small solder joint with large solder joint, the SEM micrographs of top view of IMC layer of Sn–3.0Ag–0.5Cu–0.1TiO_2 solder joints for Cu substrate are taken, as shown in Fig. 13. Results show that if 200 µm Cu pad is replaced by larger Cu substrate, a dramatic change in the IMC morphology occurs. It can be found that no matter the reflow time is long or short, the Cu_6Sn_5 grains appears to be round shape for large Cu substrate, whereas the faced shape for the small Cu pad. This is due to the fact that the small solder joint might dissolve significantly less Cu from Cu pad to the molten solder than larger solder joint [8]. For large solder joint, it will take a longer time to approach the solution saturation. This makes the concentration of Cu at the IMC/solder interface is always close to the eutectic composition which make the Cu_6Sn_5 grains appear to be round shape.

SEM micrograph of the Cu_6Sn_5 grains in Sn–3.0Ag–0.5Cu–0.6TiO_2 solder joint reflowed for 1200 s is shown in Fig. 14. The EDX analysis at point A for a small grain in Fig. 14 is shown in Fig. 15. According to the EDX result,

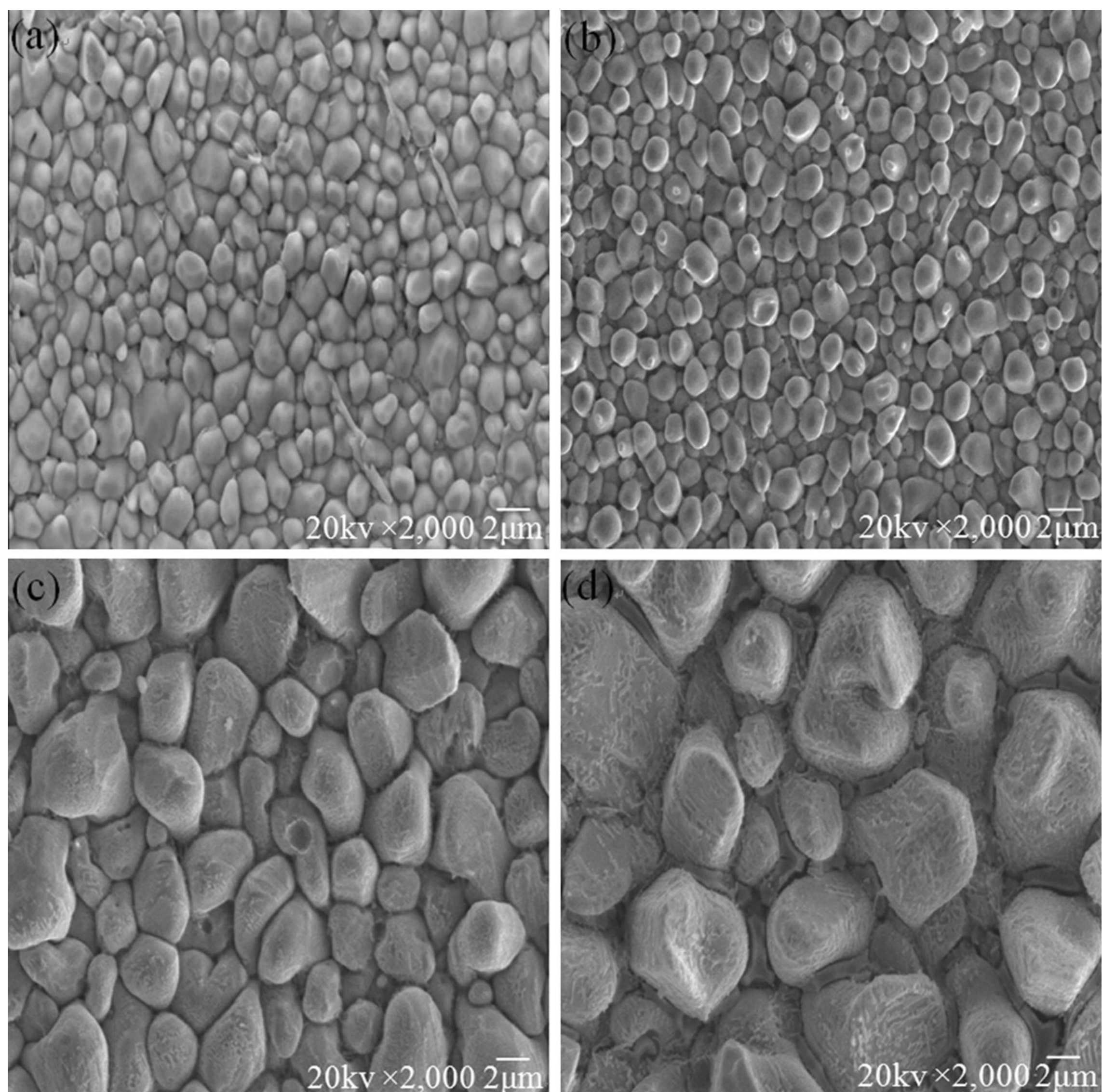

Fig. 13 SEM micrographs of top view of IMC layer of Sn–3.0Ag–0.5Cu–0.1TiO_2 solder joints reflowed for **a** 12 s, **b** 90 s, **c** 600 s and **d** 2400 s for Cu substrate [20]

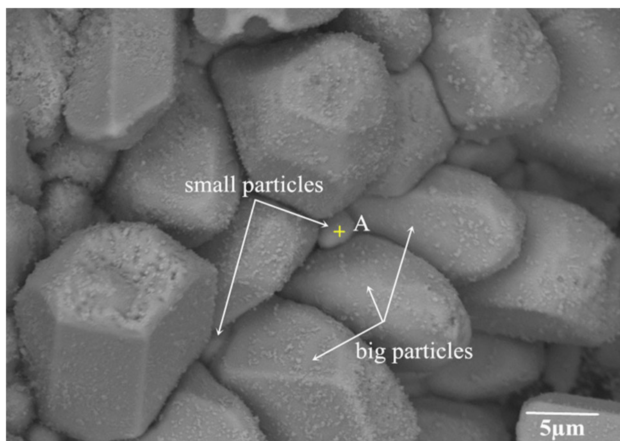

Fig. 14 SEM micrograph of the Cu_6Sn_5 grains in Sn–3.0Ag–0.5Cu–0.6TiO_2 solder joints reflowed for 1200 s for 200 μm Cu pad

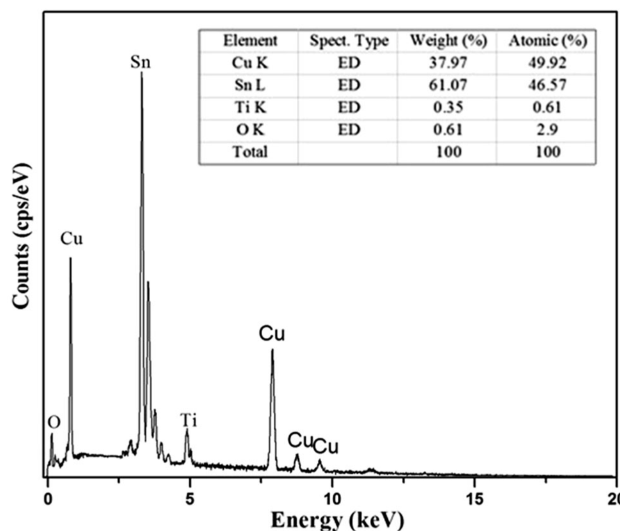

Element	Spect. Type	Weight (%)	Atomic (%)
Cu K	ED	37.97	49.92
Sn L	ED	61.07	46.57
Ti K	ED	0.35	0.61
O K	ED	0.61	2.9
Total		100	100

Fig. 15 EDX analysis at point A in Fig. 14

nano-TiO_2 might be exist in the Cu_6Sn_5 grain. During soldering reaction, TiO_2 nano-particles may be finely dispersed in the molten solder. And then some of them precipitate on the top of the substrate and become the heterogeneous nucleation sites of Cu_6Sn_5 IMC. According to the classical heterogeneous nucleation theory, the Cu_6Sn_5 phase prefers to nucleate on the TiO_2 surface in order to reduce the thermodynamic barrier [20, 28]. With the addition of TiO_2 nanoparticles, more nucleation sites are produced and the IMC nucleation rate increases. The increase in nucleation probability of Cu_6Sn_5 grains consequently leads to preventing the sequential grain ripening of the IMC grains. As a result, the addition of the TiO_2 nano-particles might result in the refinement of the grains in the TiO_2-containing solder joint.

The IMC grain size distributions in the solder joints with different TiO_2 compositions for the reflow dwell time of

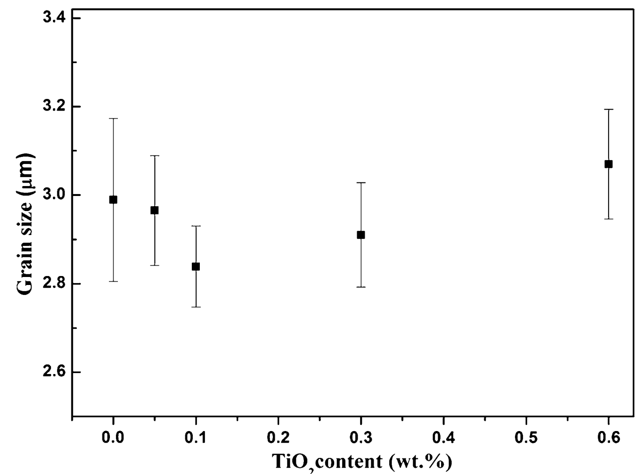

Fig. 16 IMC grain size distributions for different TiO_2 compositions reflowed for 60 s

60 s are shown in Fig. 16. It shows that the grains of TiO_2-containing solder joints are more uniform and evenly distributed than those of TiO_2-free solder joints, as discussed earlier. Under isochronal conditions, for the samples reflowed for 60 s, the average grain size in TiO_2-free solder joints is 2.98 μm, while in 0.1 wt% TiO_2-containing solder joints it decreases to 2.83 μm. In terms of the experimental results, it can be concluded that the TiO_2 additive may act as a grain refiner in IMC formation and growth. The addition of TiO_2 nano-particles may be adsorbed at the grain boundary and changes relative relationship of the growth velocities between crystalline directions of the IMC particles, which could reduces the IMC particles size [20, 28, 34]. The results reveal that the grain refining effect is most prominent when the amount of TiO_2 increases to about 0.1 wt% which shows a similar trend as the IMC thickness study. A further increase in TiO_2 proportion will cause the grain size to increase slightly. However, comparing with larger size solder joints, the IMC grain size in solder joint of 200 μm is bigger than the larger solder joint. The average IMC grain sizes of the TiO_2 free and 0.1 wt%-containing solder joints are decreases from 2.04 to 1.89 μm [16]. As well known, the size of IMC grain plays an important role in controlling the mechanical properties of the solder joints. Hence, prevention of excessive interfacial IMC growth in solder joints has become an important issue.

4 Conclusion

Effects of nano-particle TiO_2 addition on the interfacial reaction in Sn–3.0Ag–0.5Cu solder joints were studied. The microstructure and kinetics of IMC growth of the small solder joints were investigated. The main conclusions are summarized as bellow:

1. The downsizing of solder joints resulted in thicker interfacial IMC layer growth and larger interfacial Cu_6Sn_5 grains. The IMC morphologies of Sn–3.0Ag–0.5Cu solder joints have been changed as a result of TiO_2 nano-particles addition. The IMC layer becomes thinner and the grain size becomes smaller after TiO_2 addition. The optimized concentration of the TiO_2 nano-particles is found to be about 0.1 wt%.
2. The exponents for IMC layer growth in small solder joints suggest that the IMC growth kinetics does not simply obey the interfacial reaction-controlled growth or diffusion-controlled growth, but is a combination of both, which is similar to the big solder joints.
3. As the reflow time increases from 30 to 1200 s, the Cu_6Sn_5 grains firstly became more faceted in shape and then gradually become rounded. This is quite different from the case of the large size Cu/solder interface, where the top view of Cu_6Sn_5 grains appears to be round shape no matter the reflow time is long or short. The reason might be due to the change in interfacial energy between the molten solder and Cu_6Sn_5. When the composition is far away from the eutectic composition, the anisotropic interfacial energy makes the scallop morphology to be highly faceted.

Acknowledgments This research is supported by the Planned Science and Technology Project of Guangdong Province, China (No. 2013B010403003). The authors would like to acknowledge the support of the National Natural Science Foundation of Guangdong, China (No. 2014A030313594), and the Planned Science and Technology Project of Guangdong Province, China (No. 2015A020209179).

References

1. P. Hedge, D.C. Whalley, V.V. Silberschmidt, in *European Microelectronics and Packaging Conference* (IEEE, Rimini, 2009), pp. 1–9
2. A. Lalonde et al., J. Electron. Mater. **33**, 1545 (2004)
3. L.M. Yin, W.Y. Li, S. Wei, Z.L. Xu, in *12th International Conference on Electronic Packaging Technology and High Density Packaging* (IEEE, Shanghai, 2011), pp. 832–834
4. S.C. Yang, C.C. Chang, M.H. Tsai, C.R. Kao, J. Alloys Compd. **499**, 149 (2010)
5. M.N. Islam, A. Sharif, Y.C. Chan, J. Electron. Mater. **34**, 143 (2005)
6. A. Sharif, Y.C. Chan, R.A. Islam, Mater. Sci. Eng. B **106**, 120 (2004)
7. Y.S. Park, et al., in *Proceedings of the 60th Electronic Components and Technology Conference* (IEEE, Nevada, 2010), pp. 1436–1441
8. M.L. Huang and F. Yang, Sci. Rep.UK **4**, 7117, (2014)
9. L. Yin, S. Wei, Z. Xu, Y. Geng, J. Mater. Sci. Mater. Electron. **24**, 1369 (2013)
10. Y. Tang, G.Y. Li, Y.C. Pan, Mater. Des. **55**, 574 (2014)
11. T. Fouzder et al., J. Alloys Compd. **509**, 1885 (2011)
12. J. Shen, Y.C. Liu, D.J. Wang, H.X. Gao, J. Mater. Sci. Technol. **22**, 529 (2006)
13. H. Mavoori, S. Jin, J. Electron. Mater. **27**, 1216 (1998)
14. L.C. Tsao et al., Mater. Des. **31**, 4831 (2010)
15. L.C. Tsao, S.Y. Chang, Mater. Des. **31**, 990 (2010)
16. Y. Tang, G.Y. Li, D.Q. Chen, Y.C. Pan, J. Mater. Sci. Mater. Electron. **25**, 981 (2014)
17. N.M. Nasir et al., Mater. Sci. Forum **803**, 273 (2014)
18. Y. Tang et al., J. Mater. Sci. Mater. Electron. **26**, 3196 (2015)
19. A.K. Gain, Y.C. Chan, W.K.C. Yung, Microelectron. Reliab. **51**, 975 (2011)
20. Y. Tang, G.Y. Li, Y.C. Pan, J. Alloys Compd. **554**, 195 (2013)
21. L.C. Tsao, M.W. Wu, S.Y. Chang, J. Mater. Sci. Mater. Electron. **23**, 681 (2012)
22. C.C. Chang, Y.W. Lin, Y.W. Wang, C.R. Kao, J. Alloys Compd. **492**, 99 (2010)
23. K. Zeng et al., J. Appl. Phys. **97**, 24508 (2005)
24. J. Shen, Y.C. Chan, Microelectron. Reliab. **49**, 223 (2009)
25. Y. Li, Y.C. Chan, J. Alloys Compd. **645**, 566 (2015)
26. L.C. Tsao, J. Alloys Compd. **509**, 2326 (2011)
27. S. Chada, W. Laub, R.A. Fournelle, D. Shangguan, J. Electron. Mater. **28**, 1194 (1999)
28. G.Y. Li, B.L. Chen, J.N. Tey, IEEE Trans. Electron. Packag. Manuf. **27**, 77 (2004)
29. T. Laurila, V. Vuorinen, J.K. Kivilahti, Mater. Sci. Eng. R **49**, 1 (2005)
30. K.W. Moon et al., J. Electron. Mater. **29**, 1122 (2000)
31. C.K. Wong et al., Microelectron. Reliab. **48**, 611 (2008)
32. J.O. Suh, K.N. Tu, G.V. Lutsenko, A.M. Gusak, Acta Mater. **56**, 1075 (2008)
33. K.N. Tu, A.M. Gusak, M. Li, J. Appl. Phys. **93**, 1335 (2003)
34. A.K. Gain, Y.C. Chan, W.K.C. Yung, Microelectron. Reliab. **51**, 2306 (2011)